Available online at www.sciencedirect.com
SCIENCE DIRECT®
International Journal of Heat and Mass Transfer 48 (2005) 2708–2721
International Journal of HEAT and MASS TRANSFER
www.elsevier.com/locate/ijhmt

Unsteady turbulent heat transfer of mixed convection in a reciprocating circular ribbed channel

Horng-Wen Wu *, Chin-Teck Lau

Department of System and Naval Mechatronic Engineering, National Cheng Kung University, Tainan 701, Taiwan, ROC

Received 18 May 2004; received in revised form 31 January 2005
Available online 21 March 2005

Abstract

The SIMPLE-C scheme is used to solve the mass, momentum, energy conservation equations and turbulent k–ε equations with a two-layer model near wall for a fluid past a reciprocating circular ribbed channel when changing Reynolds number (4250–10,000), Grashof number (0–400,000,000), pulsating number (0–9.3) and cooling mediums. The average time-mean Nusselt number for the reciprocating circular ribbed channel can be 45–182% larger than that for the equivalent stationary smooth channel. The heat transfer enhancement produced by buoyancy for the reciprocating circular ribbed channel decreases as the pulsating number increases. The oscillating amplitude of Nusselt number with crank angle in the oil-cooling is less than in the water-cooling.

Keywords: Unsteady turbulent heat transfer; Mixed convection; A reciprocating circular ribbed channel

1. Introduction

The possibility of enhancing the heat transfer rate from piston has been explored by means of cooling channels in marine heavy engines such as diesel engines and Stirling engines in order to obtain low fuel consumption and high power [1,2]. The fluid flow and heat transfer within the cooling channels are very complicated because the pressurized water or oil in these channels has to reciprocate with the piston. Despite the heat transfer enhancement devices for the cooling channels, the effect of the reciprocation motion on the heat transfer has to be considered.

Chang and Su [3] conducted an experimental work on the heat transfer from a reciprocating square ribbed enclosure. They found that at the highest reciprocating speed test, the heat transfer enhancement due to the pure shaking effect is 45% of the equivalent stationary situation. However, relatively few investigations have been performed on this kind of study, but the similar study is on pulsating or oscillatory flow superimposed for a stationary channel. Mackley et al. [4] conducted experimental heat transfer measurements for smooth and baffled tubes with flow oscillations superimposed on the net flow, and reported a significant increase in the Nusselt number for the baffled tube. Howes and Mackley [5] presented a simulation of chaotic mixing and dispersion for baffled channels, within which a periodic flow was forced with or without a net through-flow. They found that a

* Corresponding author. Tel.: +886 6 274 7018; fax: +886 6 274 7019.
E-mail address: z7708033@email.ncku.edu.tw (H.-W. Wu).

0017-9310/$ - see front matter © 2005 Elsevier Ltd. All rights reserved.
doi:10.1016/j.ijheatmasstransfer.2005.01.014

Nomenclature

C_1, C_2, C_3	constants in turbulent model
D	diameter of a circular ribbed channel
E	empirical coefficient used for the wall function
G_k	generation rate of turbulent kinetic energy
Gr	Grashof number ($Gr = g\beta q_w D^4/(Kv^2)$)
H	distance from entrance to first rib or rib spacing
h	rib width
K	thermal conductivity
k	turbulence kinetic energy
L	length of a circular ribbed channel
l_c	connecting rod length
l_μ, l_ε	length-scales ($l_\mu = C_1 y[1-\exp(-Re_y/A_\mu)]$, $l_\varepsilon = C_1 y/(1+5.3/Re_y)$)
Nu	local Nusselt number ($\partial T/(T_w \partial n)$)
$\overline{Nu}$	time-averaged Nusselt number
n	normal vector
P	dimensionless pressure ($P^*/\rho U_m^2$)
Pr	Prandtl number (v/α)
Pr_t	turbulent Prandtl number (v_t/α_t)
Pu	pulsating number ($\omega R_{cr}/U_m$)
q_w	heat flux at the channel wall
R_{cr}	radius of crankshaft
Re	Reynolds number ($U_m D/v$)
Re_e	effective Reynolds number ($1/Re + 1/Re_t$)
Re_t	turbulence Reynolds number ($U_m D/v_t$)
Re_y	turbulence Reynolds number near the wall ($\sqrt{k}y/v$)
r, z, θ	dimensionless cylindrical coordinates relative to the stationary coordinate system
$\tilde{r}$, $\tilde{z}$, $\tilde{\theta}$	dimensionless cylindrical coordinates relative to the reciprocating system coordinate ($\tilde{r} = \tilde{r}^*/D$, $\tilde{z} = \tilde{z}^*/D$, $\tilde{\theta} = \tilde{\theta}^*$)
S_Φ	source term for variable
$\tilde{t}$	dimensionless time ($\tilde{t}^*/(D/U_m)$)
T	dimensionless temperature ($(T^* - T_\infty)/(q_w D/K)$)
U, V	dimensionless axial and radial velocity components in the stationary frame
u, v	dimensionless axial and radial relative velocity components in the reciprocating frame ($u = u^*/U_m$, $v = v^*/U_m$)
U_m	inlet velocity
U_P	dimensionless piston speed ($U_P = Pu\sin(\omega t^*)\{-1+\cos(\omega t^*)/[(l_c/R)^2 - \sin^2(\omega t^*)]^{\frac{1}{2}}\}$)
U_P^*	piston speed
w	rib height
y	minimum distance to the wall
Γ_Φ	turbulent diffusion coefficient
∇	del, a vector operator
∇^2	Laplacian operator
Φ	dependent variable
κ	von Kármán constant
ε	turbulence dissipation rate
σ_k, σ_ε	constants in turbulent model
ρ	fluid density
v	kinematic viscosity of fluid
v_t	turbulent kinematic viscosity of fluid
ω	revolving velocity
τ_w	wall shear stress

Superscript

*	dimensional physical quantity

Subscripts

0	initial location
w	wall
∞	reference
s	surface-averaged for smooth channel
ave	surface-averaged

baffled channel could generate a well-mixed flow. Fusegi [6] performed numerical computations on the fully developed turbulent flow and heat transfer in a periodically ribbed channel with an externally sustained oscillatory pressure gradient. His results showed that eminent vortical structure has significant bearing on the heat transfer rate at the constant-heat-transfer surface at the lower wall of the channel. Fusegi [7] also investigated the combined effects of the oscillatory through-flow and the buoyancy on the heat characteristics of a laminar flow in a periodically grooved channel.

However, *there are no numerical studies available on turbulent buoyant flow and heat transfer in a circular ribbed channel undergoing reciprocating motion*. This paper uses a SIMPLE-C method of Van Doormaal and Raithby [8] and k–ε turbulent model [9] with a two-layer model near wall [10] to investigate the turbulent buoyant flow generated in reciprocating motion and its effect on heat transfer along the wall surface. For the purpose of effectively solving this problem, velocity components in the stationary frame has to be changed to the relative velocity components in the reciprocating frame as the procedure Sabersky et al. [11] used to solve the rotation problem of a turbine.

The objective of this paper is to quantify the effect of Reynolds number, Grashof number and pulsating number on heat transfer from a circular ribbed channel at constant wall heat flux when the channel is in the process

of reciprocating motion for cooling fluids including water and oil. The results of this study may be of interest to engineers attempting to design piston cooling in heavy engines and to researchers interested in the flow-management aspect of heat transfer enhancement by means of ribs embedded in a reciprocating circular channel.

2. Mathematical model

Fig. 1 shows the configuration enclosing the flow domain considered in the present study. It is assumed to be an axisymmetric turbulent flow in a circular ribbed channel on the simplified piston undergoing reciprocating motion. The Navier–Stokes equations, energy equation and the k–ε turbulent models [9] are employed here. The geometrical relations for this ribbed channel are set as $L/D = 10$, $H/D = 1$, $w/D = 0.1$, and $h/w = 1$. In order to simplify the turbulent flow phenomena in pipe, the following assumptions are made: (1) the fluid is incompressible; (2) no-swirling flow; (3) all the fluid properties are assumed to be constant; (4) the turbulent viscosity coefficient is isotropic; (5) Boussinesq approximation is available for the buoyancy effect [12]. To describe the fluid motion inside the reciprocating cooling passage, we employ a new coordinate system which itself is in reciprocating motion. Fig. 1 shows the relation between two coordinates systems. If (U^*, V^*) be the velocity components in the stationary frame (r^*, z^*, θ^*), and (u^*, v^*) be the relative velocity components in the reciprocating frame $(\tilde{r}^*, \tilde{z}^*, \tilde{\theta}^*)$, we can write

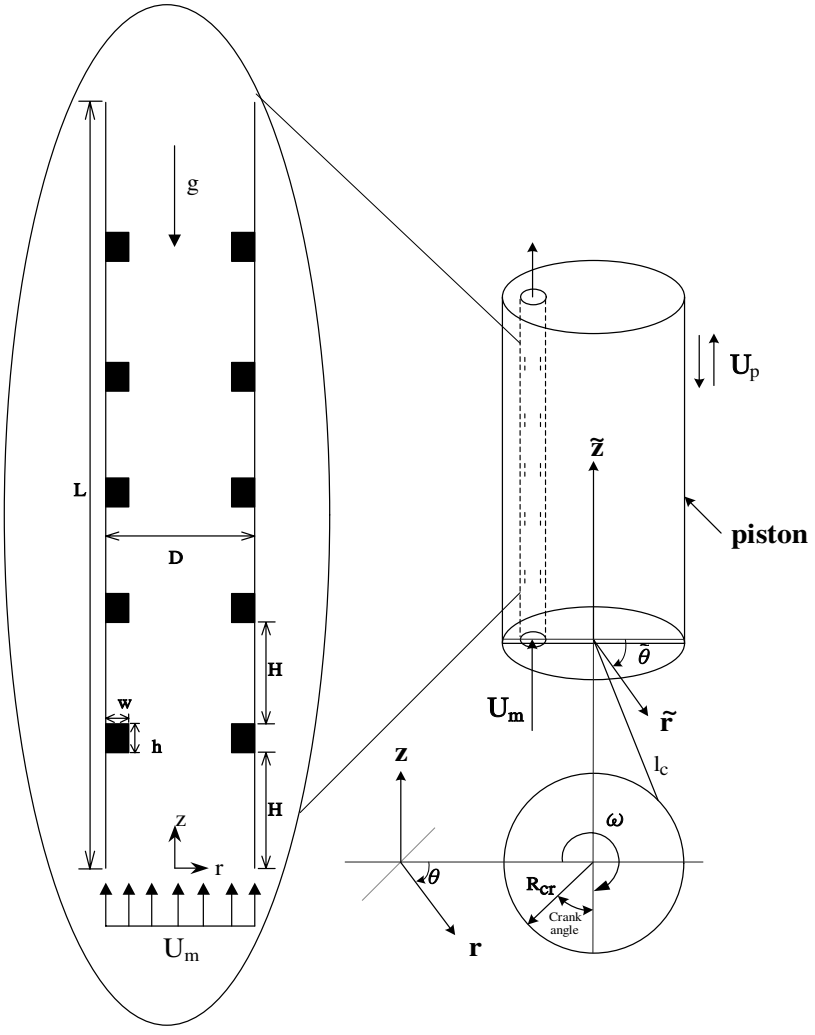

Fig. 1. A circular ribbed channel on a reciprocating piston.

$$U^* = u^* + U_P^*$$
$$V^* = v^* \quad (1)$$

In which piston velocity is equal to

$$U_P^* = \omega R_{cr} \sin(\omega t^*) \left\{ -1 + \frac{\cos(\omega t^*)}{\left[\left(\frac{l_c}{R_{cr}} \right)^2 - \sin^2(\omega t^*) \right]^{\frac{1}{2}}} \right\} \quad (2)$$

The relative positions of the reciprocating system with respect to the stationary frame are

$$\tilde{t}^* = t^*$$
$$\tilde{r}^* = r^* - r_0^*$$
$$\tilde{\theta}^* = \theta^* - \theta_0^* \quad (3)$$
$$\tilde{z}^* = z^* - z_0^* - \int_0^{t^*} U_P^*(\tau)\,\mathrm{d}\tau$$

May yield

$$\frac{\partial}{\partial t^*} = \frac{\partial}{\partial \tilde{t}^*} - U_P^* \frac{\partial}{\partial \tilde{z}^*} \quad (4)$$

$$\nabla = \tilde{\nabla}, \quad \nabla^2 = \tilde{\nabla}^2 \quad (5)$$

After substituting Eqs. (1)–(5) into the momentum and energy equations, we can get a new set of the governing equations in the reciprocating frame after the coordinate transformation. Introducing the following non-dimensional parameters

$$\tilde{r} = \frac{\tilde{r}^*}{D}, \quad \tilde{z} = \frac{\tilde{z}^*}{D}, \quad \tilde{t} = \frac{\tilde{t}^*}{D/U_m}$$
$$u = \frac{u^*}{U_m}, \quad v = \frac{v^*}{U_m}, \quad T = \frac{T^* - T_\infty}{\frac{q_w D}{K}}$$
$$P = \frac{P^*}{\rho U_m^2}, \quad k = \frac{k^*}{U_m^2}, \quad \varepsilon = \frac{\varepsilon^*}{U_m^3/D}$$
$$Re = \frac{U_m D}{\nu}, \quad Re_t = \frac{U_m D}{\nu_t}, \quad Gr = \frac{g\beta q_w D^4}{K\nu^2}, \quad Pu = \frac{\omega R_{cr}}{U_m} \quad (6)$$

Consequently, for the axisymmetric flow the general form of the dimensionless governing equations can be expressed as follows:

$$\frac{\partial(\rho\Phi)}{\partial\tilde{t}} + \frac{1}{\tilde{r}}\left[\frac{\partial}{\partial\tilde{r}}(\tilde{r}\rho v\Phi) + \frac{\partial}{\partial\tilde{z}}(\tilde{r}\rho u\Phi)\right] = \frac{1}{\tilde{r}}\left[\frac{\partial}{\partial\tilde{r}}\left(\tilde{r}\Gamma_\Phi\frac{\partial\Phi}{\partial\tilde{r}}\right) + \frac{\partial}{\partial\tilde{z}}\left(\tilde{r}\Gamma_\Phi\frac{\partial\Phi}{\partial\tilde{z}}\right)\right] + \widetilde{S}_\Phi \quad (7)$$

where Φ is the dependent variable. In the left-hand side, the first term represents the unsteady term and the second term represents the convective effect of the flow field so-called convection term. The first term in the right-hand side represents the diffusive effect and so-called diffusion term. $\widetilde{S}_\Phi$ and Γ_Φ are the source term and turbulent diffusion coefficient, respectively. The corresponding Φ, Γ_Φ and $\widetilde{S}_\Phi$ in every conservative equation and the turbulent empirical constants Launder and Spalding [9] used are listed in Table 1.

Table 1
Diffusion coefficients and source terms with parameters expression in governing equations

Φ	Γ_Φ	$\widetilde{S}_\Phi$
1	0	0
u	$\frac{1}{Re_e}$	$-\frac{\partial P}{\partial\tilde{z}} + \frac{1}{\tilde{r}}\frac{\partial}{\partial\tilde{r}}\left(\tilde{r}\frac{1}{Re_e}\frac{\partial v}{\partial\tilde{z}}\right) + \frac{\partial}{\partial\tilde{z}}\left(\frac{1}{Re_e}\frac{\partial u}{\partial\tilde{z}}\right) - \frac{2}{3}\frac{\partial k}{\partial\tilde{z}} + \frac{Gr}{Re^2}T - \frac{\partial(\rho U_p)}{\partial\tilde{t}}$
v	$\frac{1}{Re_e}$	$-\frac{\partial P}{\partial\tilde{r}} + \frac{1}{\tilde{r}}\frac{\partial}{\partial\tilde{r}}\left(\tilde{r}\frac{1}{Re_e}\frac{\partial v}{\partial\tilde{r}}\right) + \frac{\partial}{\partial\tilde{z}}\left(\frac{1}{Re_e}\frac{\partial u}{\partial\tilde{r}}\right) - \frac{2}{Re_e}\frac{v}{\tilde{r}^2} - \frac{2}{3}\frac{\partial k}{\partial\tilde{r}}$
k	$\frac{1}{Re} + \frac{1}{Re_t}\frac{1}{\sigma_k}$	$G_k - \rho\varepsilon - \frac{Gr}{Pr_t Re_t Re^2}\frac{\partial T}{\partial\tilde{z}}$
ε	$\frac{1}{Re} + \frac{1}{Re_t}\frac{1}{\sigma_\varepsilon}$	$\frac{\varepsilon}{k}\left(C_1 G_k - C_2\varepsilon - C_3\frac{Gr}{Pr_t Re_t Re^2}\frac{\partial T}{\partial\tilde{z}}\right)$
T	$\frac{1}{PrRe} + \frac{1}{Pr_t Re_t}$	0

Note:

$$G_k = \frac{1}{Re_t}\left\{2\left[\left(\frac{\partial u}{\partial\tilde{z}}\right)^2 + \left(\frac{\partial v}{\partial\tilde{r}}\right)^2 + \left(\frac{v}{\tilde{r}}\right)^2\right] + \left(\frac{\partial v}{\partial\tilde{z}} + \frac{\partial u}{\partial\tilde{r}}\right)^2\right\}.$$

$$\frac{1}{Re_e} = \frac{1}{Re} + \frac{1}{Re_t}.$$

$\sigma_k = 1.0 \quad \sigma_\varepsilon = 1.3 \quad Pr_t = 0.9.$

$C_1 = 1.44 \quad C_2 = 1.92 \quad C_3 = 0.7.$

For the two-dimensional and geometric symmetry, the boundary conditions at the inlet, outlet, and symmetric axis and the wall are prescribed in the present study.

(1) Inlet:

$$u = 1 - U_P, \quad v = 0, \quad T = 0$$

$$k = 0.003u^2, \quad \varepsilon = C_\mu k^{1.5}/0.015 \quad [13] \tag{8}$$

(2) Outlet:
The diffusion coefficient is assumed to be small at outflow boundary condition [14].

(3) Symmetric axis:

$$\frac{\partial \Phi}{\partial \tilde{r}} = 0, \quad v = 0, \quad \text{where } \Phi = u, k, \varepsilon, T \tag{9}$$

(4) Walls channel (including ribs):

$$u = 0, \quad v = 0$$

$$\frac{\partial T}{\partial n} = -1 \quad \text{(Constant heat flux)} \tag{10}$$

In which n denotes the normal to the solid surface. Then the local Nusselt number (Nu) may be defined as

$$Nu = \frac{1}{T_w}\frac{\partial T}{\partial n} \tag{11}$$

In order to save grid points and hence computer storage and time, to increase the robustness of the method, and also to introduce the fairly well length-scale established distribution very near walls into the model, the present study applies two-layer model. That is, use k–ε models only away from the wall and the near-wall, viscous-affected regions are resolved with a one-equation turbulence model; that is, turbulent kinetic energy k is determined from the model while its dissipation rate ε is determined from a prescribed length-scale distribution l. Hence, the eddy viscosity relation is rewritten as

$$\mu_t = \rho C_\mu \sqrt{k} l_\mu \tag{12}$$

and ε is determined from

$$\varepsilon = \frac{k^{\frac{3}{2}}}{l_\varepsilon} \tag{13}$$

The length-scales l_μ and l_ε adopted by Rodi [10] is from the length-scale model of Norris and Reynolds [15] because the Norris-Reynolds model was found to perform well in boundary layers with an adverse pressure gradient and transpiration. The length-scales relation employ is presented as follows:

$$l_\mu = C_l y\left[1 - \exp\left(-\frac{Re_y}{A_\mu}\right)\right] \tag{14}$$

$$l_\varepsilon = \frac{C_l y}{1 + 5.3/Re_y} \tag{15}$$

which involves the argument Re_y defined as $Re_y = \frac{\sqrt{k}y}{\nu}$. Re_y varies relatively slowly along lines parallel to the wall, does not vanish at separation, and remains well defined in the regions of flow reversal. The constant C_l is chosen as $C_l = \kappa C_\mu^{-3/4}$, where $\kappa(= 0.41)$ is the von Kármán constant, while A_μ are model coefficients equal to 50.5 which proposed by Rodi [10].

Formulation and discretization for all transport equations are obtained by means of the SIMPLE-C algorithm with the control volume approach for each equation arranged into transient, diffusion, convection, and source terms.

3. Results and discussion

In this study, the Reynolds numbers are taken as 5000, 8000 and 10,000, the Grashof numbers as 0, 10,000,000, and 400,000,000 and the pulsating numbers as 0, 1.55, 1.94, 3.1, 3.87, 4.64, 5.8 and 9.3 when the Prandtl number is kept at 7.0 for water and at 84 for cooling oil. All the calculations have been performed by using K7-500 computer. A mesh (205×52) was chosen for all cases after several test runs have been made. Further refinement changed the Nusselt number less than 0.05% for the test runs. The other two meshes tested are 190×40 and 224×66. The time increment $\Delta\tilde{t}$ was set at 0.001 in the calculations of unsteady flow and heat transfer to keep Courant number less than 1, and the computation time was about 18 hr to 20 hr of CPU time. Since there were no suitable reports found to deal with a circular ribbed channel heated under reciprocating motion, we apply the present method to solve turbulent flow in a stationary rib-roughened circular tube at Re = 10,000, Pr = 0.73 before solving the problem. The rib-roughened circular tube wall is considered to be at a uniform heat flux. As shown in Fig. 2, the trend of time-averaged Nusselt number agrees well with Kiml et al.'s experimental results [16], although the maximum difference between the numerical and experimental values is 8%. Hence it still gives one confidence in the use of the present solution scheme.

Because the channel moves at variable speed up and down, the flow field in the channel is subject to a reciprocating force resulting in flow acceleration or deceleration. Stream patterns for the third to fifth ribs in a circular ribbed channel are shown in Fig. 3 for different crank angle, at Re = 5000, Gr = 0, Pu = 6.2 and Pr = 7.0, where the cooling fluid is water. The fluid movement in the channel is from left to right due to inertia of fluid when piston speed is zero at 0°. Two recirculation zones are also generated between two ribs, and one generated in front of each rib becomes larger and obviously combines with another in rear of each rib to form a single one from

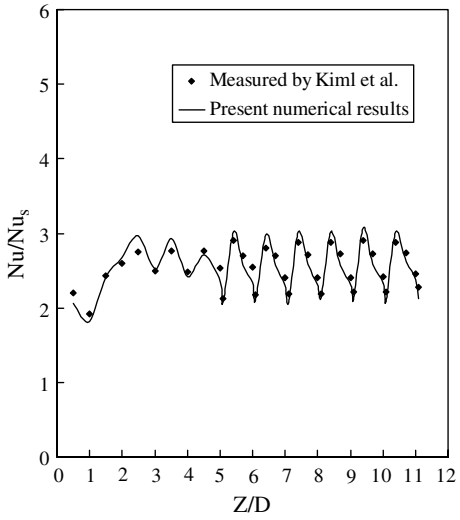

Fig. 2. Comparison between the present predictions and Kiml et al.'s predictions for a stationary rib-roughened circular tube with uniform wall heat flux at $Re = 10{,}000$ and $Pr = 0.73$.

30° to 80°. This result is due to a reversing flow when piston moves from bottom dead center towards top dead center and piston speed is larger than fluid speed at the inlet. The recirculation zone is generated in front of each rib, and it becomes larger from 200° to 280° with an increase in positive relative velocity; since piston speed increases and both piston and fluid speed at the inlet are in the opposite direction when piston moves from top dead center towards bottom dead center. When the pulsating number increases to 9.3, stream patterns for the third to fifth ribs in a circular ribbed channel are indicated in Fig. 4. The recirculation zone in front of each rib in Fig. 4 is larger than that of the corresponding rib in Fig. 3 for the crank angle due to the increased reciprocating force except at 0°. Figs. 5 and 6 show the transient Nusselt numbers along the circular ribbed channel wall for a reciprocating circular ribbed channel at $Pu = 6.2$ (60 rpm) and $Pu = 9.3$ (90 rpm) for $Pr = 7.0$, $Re = 5000$, and $Gr = 0$. The transient Nusselt numbers for both Figs. 5 and 6 have the same trend along the circular ribbed channel wall and periodical variation with crank angle because the fluid in the channel is subject to the periodical reciprocating force due to the reciprocating motion of piston like sine wave one; besides, these values and the amplitudes of oscillations increase as the pulsating number increases. For the same Reynolds number, a larger pulsating number denotes a larger revolving speed of crankshaft by its definition; this larger revolving speed can make relative velocity between the fluid and the channel vary periodically with shorter period and larger amplitude of oscillation so as to obtain such a Nusselt number distribution. However, the maximum values of Nusselt number occur at the front corner of the each rib; the minimum values occur at the regions near both the front and rear corners of each rib. The values of Nusselt number of the region between two ribs increase downstream to reach another maximum value and then decrease. Apparently, these phenomena for both above cases are physically reasonable. It can be explained from Figs. 3 and 4 that when flow passes over the ribs, it is locally accelerated due to the diameter of the channel decreased and the curvature of the streamline at the corner is very large to get a high speed; so the turbulent convective hear transfer is large. A recirculation zone is formed in the region near the front or rear corner of each rib so that the heat is transferred poorly to the mainstream flow. Generation of two recirculation zones between two ribs causes the variation of Nusselt number with downstream. Fig. 7 indicates the transient Nusselt number variation along the channel wall for a reciprocating circular ribbed channel with $Re = 10{,}000$, $Pr = 7.0$ and $Pu = 3.1$ (60 rpm). For the same revolving speed (60 rpm) under forced convection, Nusselt number increases as Reynolds number increases due to larger forced convection from a comparison of Fig. 7 with Fig. 5. Fig. 8 shows the transient Nusselt number variation along channel wall for a reciprocating circular ribbed channel at $Pr = 7.0$, $Re = 5000$, $Gr = 400{,}000{,}000$, and $Pu = 6.2$ (60 rpm). For the same Reynolds number and pulsating number as shown in Figs. 5 and 8, increasing Grashof number makes little difference in the variation of Nusselt number along channel wall and with crank angle. This result is due to the reciprocating force larger than the buoyancy force of fluid when the channel undergoes reciprocating motion. In addition, increasing the relative flow speed obtains effective heat transfer to even temperature variation and decreases buoyancy effect. Fig. 8 shows transient Nusselt number variation along channel wall for a reciprocating circular ribbed channel at $Pr = 7.0$, $Re = 10{,}000$, $Gr = 400{,}000{,}000$, and $Pu = 3.1$ (60 rpm). For the fixed Grashof number and revolving speed (60 rpm) as shown in Fig. 8 ($Pu = 6.2$) and Fig. 9 ($Pu = 3.1$), an increase in Reynolds number increases transient Nusselt number variation, because this reduces the value of Gr/Re^2, and then the forced convection dominates the flow-field even in the presence of the buoyancy force.

Cooling oil is also used as a coolant in practical piston cooling for a low heat rejection engine; if the same velocity of inlet fluid is applied to water and oil, $Re = 10{,}000$ is for water and $Re = 4250$ is for oil due to different viscosity. The Nusselt number variation along channel wall for a reciprocating circular ribbed channel at $Pr = 84$, $Re = 4250$, $Gr = 0$, and $Pu = 3.1$ (60 rpm) is shown in Fig. 10. The distribution of Nusselt number is smaller than the case of water-cooling for a circular ribbed channel as shown in Fig. 7; this smaller distribution is due to the smaller heat capacity for oil. Therefore, if oil cooling wants to have the same cooling

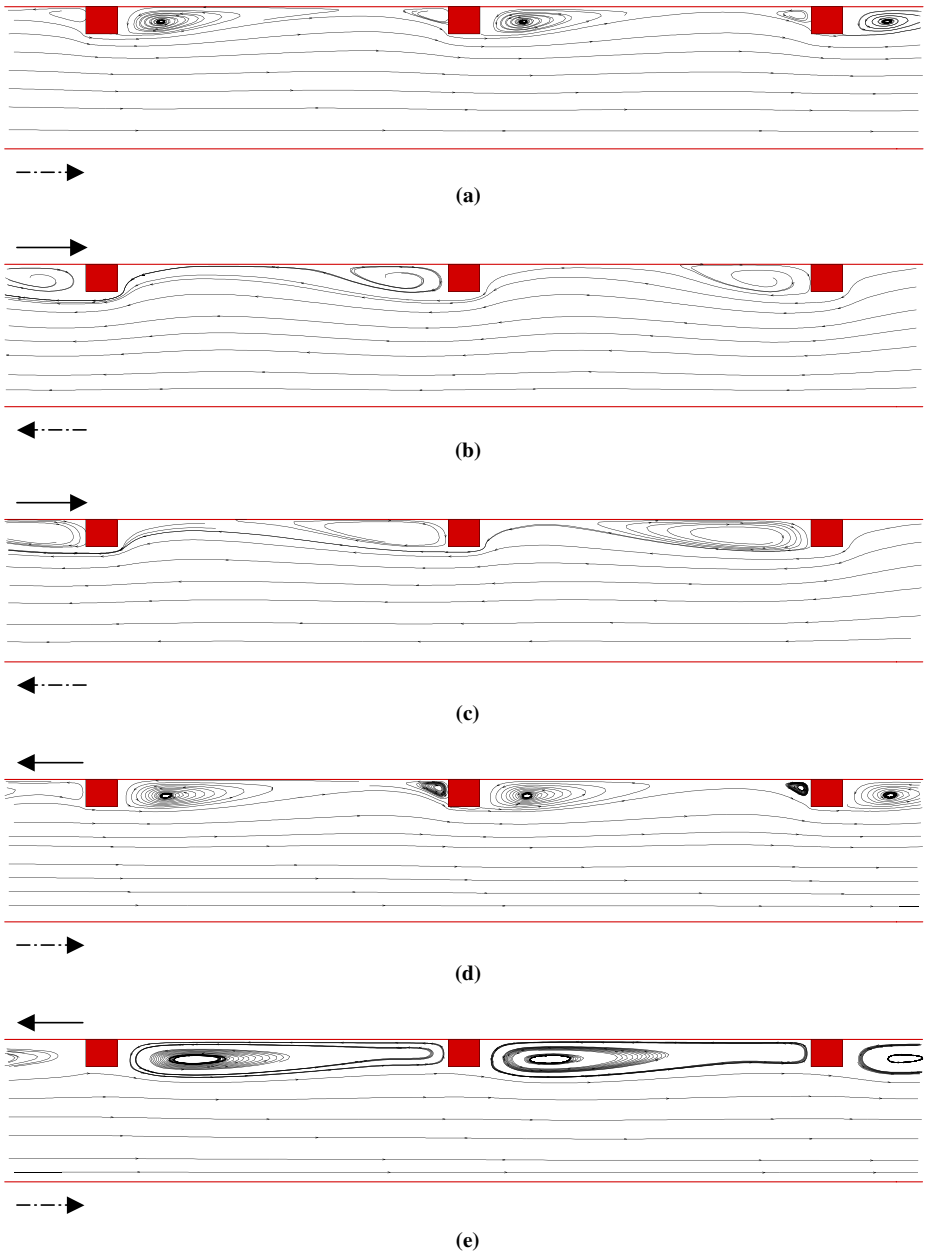

Fig. 3. Stream patterns for the third to fifth ribs in a circular ribbed channel with $Re = 5000$, $Gr = 0$, and $Pu = 6.2$ at crankshaft angle equal to (a) 0°; (b) 30°; (c) 80°; (d) 200°; (e) 280° ($Pr = 7.0$). ((——▶) piston movement direction; (–·–·–▶) fluid movement direction; the gravitation direction in all figures is from right to left.)

effect as water-cooling, it has to increase the flow rate. Fig. 10 also indicates that Nusselt number has periodical variation with crank angle but less oscillating amplitude in the oil-cooling than in the water-cooling case as shown in Fig. 7. This less oscillating amplitude can be explained by that even with the same pulsating number, the oil-cooling case has a higher Prandtl number resulting in viscous dissipation larger than heat conduction in fluid. Fig. 11 indicates transient Nusselt number variation along channel wall for a reciprocating circular ribbed channel at $Pr = 84.0$, $Re = 4250$, $Gr = 0$, and $Pu = 4.64$ (90 rpm). Like the water-cooling case, the transient Nusselt number varies along channel wall and it also increases with increasing pulsating number. Fig. 12 shows the transient Nusselt number variation along channel wall for a reciprocating circular ribbed

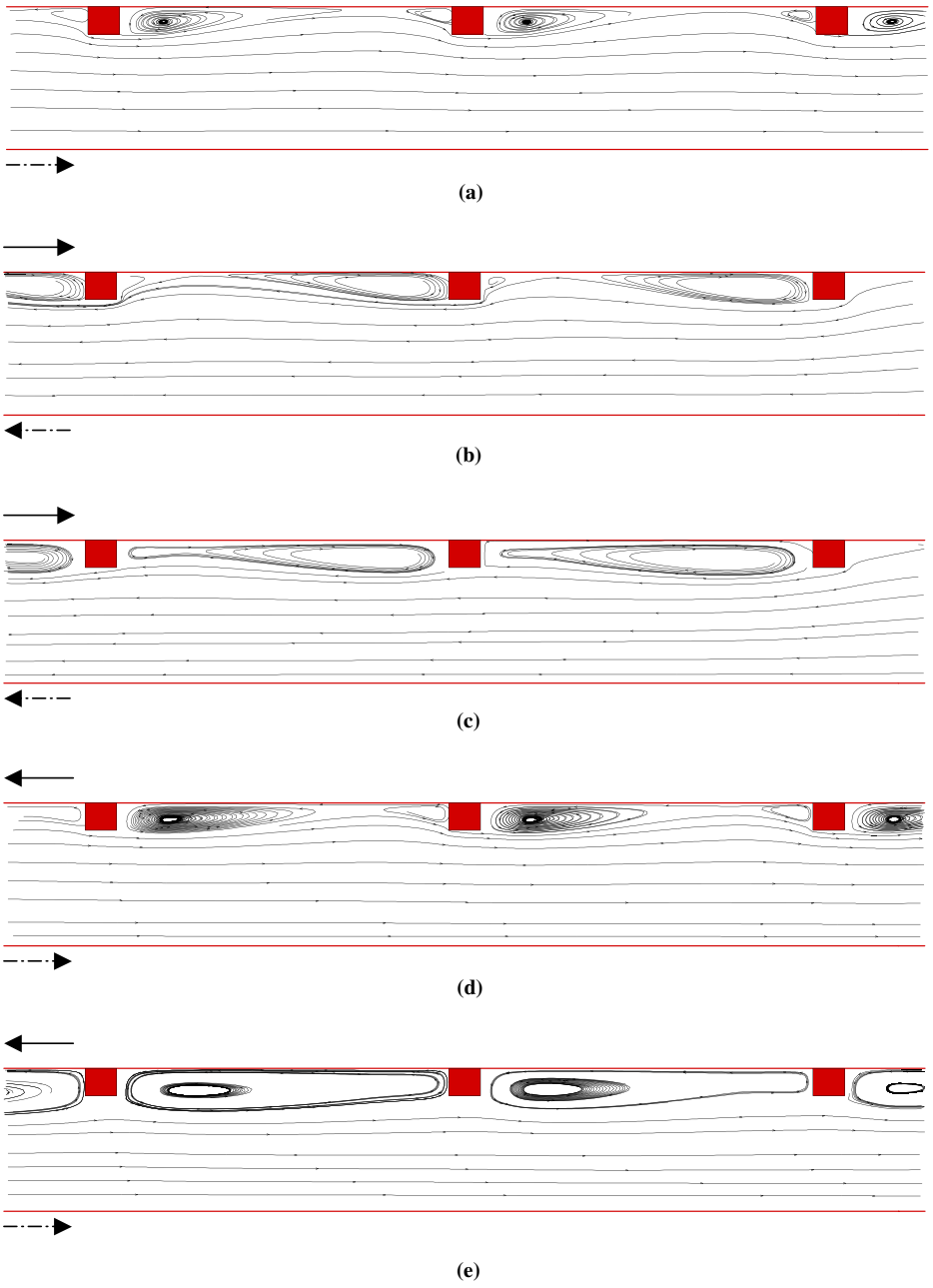

Fig. 4. Stream patterns for the third to fifth ribs in a circular ribbed channel with $Re = 5000$, $Gr = 0$, and $Pu = 9.3$ at crankshaft angle equal to (a) 0°; (b) 30°; (c) 80°; (d) 200°; (e) 280° ($Pr = 7.0$). ((——▶) piston movement direction; (–·–·–▶) fluid movement direction; the gravitation direction in all figures is from right to left.)

channel at $Pr = 84$, $Re = 4250$, $Gr = 400{,}000{,}000$, and $Pu = 3.1$ (60 rpm). Like the water-cooling case, from a comparison of Fig. 12 with Fig. 10, for the same Reynolds number and pulsating number as shown in Figs. 5 and 8, increasing Grashof number makes little difference in the variation of Nusselt number along channel wall and with crank angle.

The surface-and time-averaged Nusselt number is calculated by the values of time-averaged Nusselt number on all grids of the ribbed channel wall boundary. The values of surface-and time-averaged Nusselt number for channel at various values of Reynolds number, Grashof number and pulsating number are listed in Table 2 for cooling water and in Table 3 for cooling

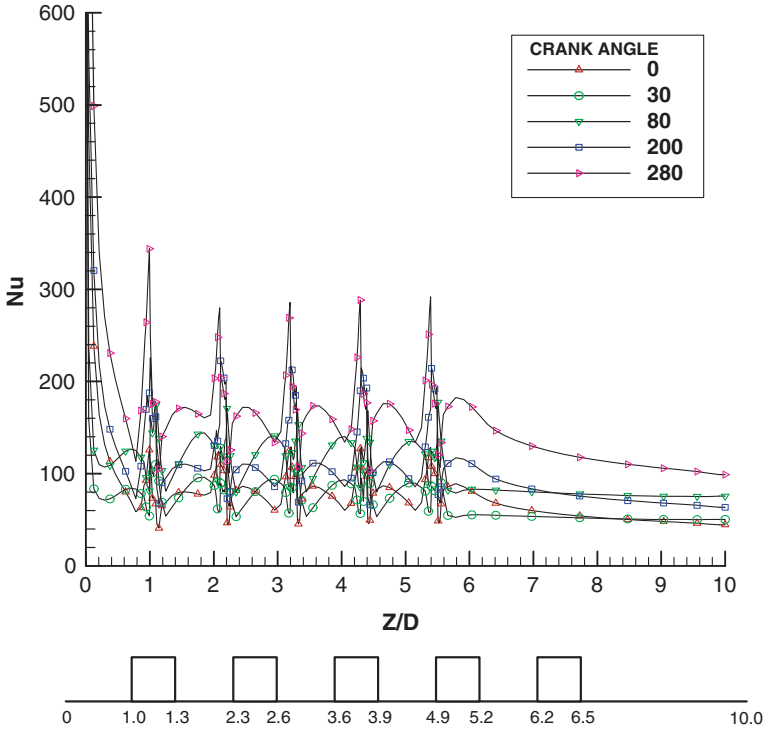

Fig. 5. Transient Nusselt number variation along channel wall for a reciprocating circular ribbed channel at $Pr = 7.0$, $Re = 5000$, $Gr = 0$, and $Pu = 6.2$ (60 rpm).

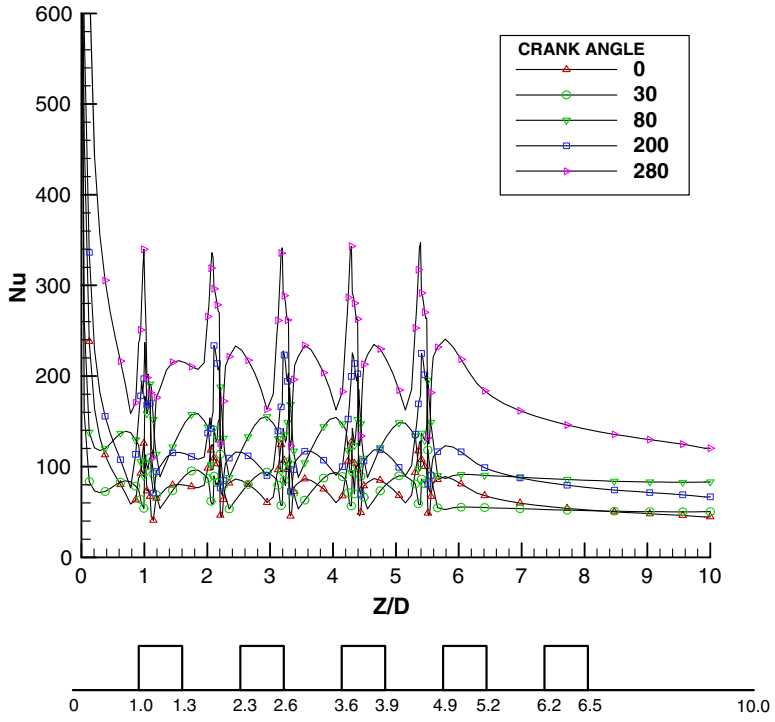

Fig. 6. Transient Nusselt number variation along channel wall for a reciprocating circular ribbed channel at $Pr = 7.0$, $Re = 5000$, $Gr = 0$, and $Pu = 9.3$ (90 rpm).

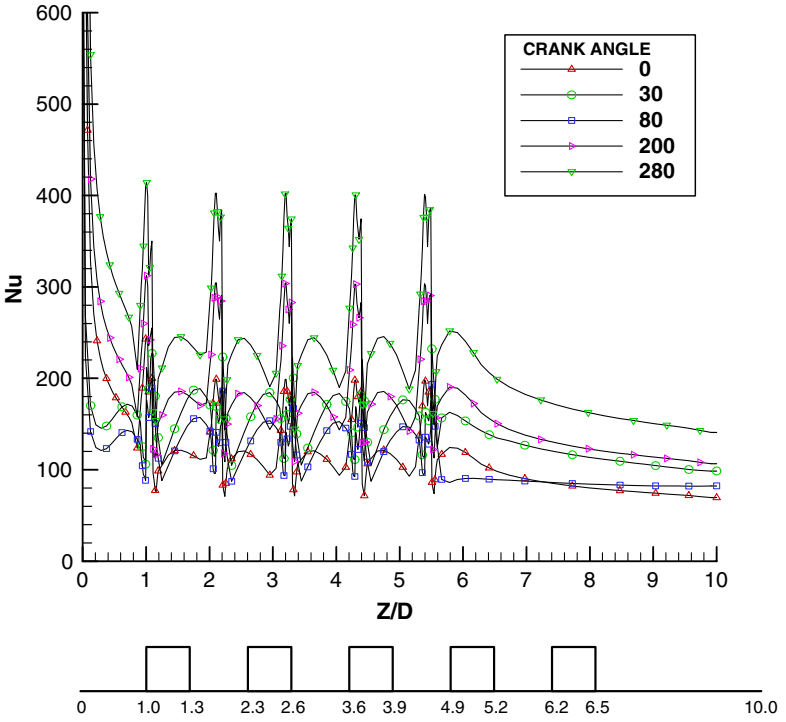

Fig. 7. Transient Nusselt number variation along channel wall for a reciprocating circular ribbed channel at $Pr = 7.0$, $Re = 10{,}000$, $Gr = 0$, and $Pu = 3.1$ (60 rpm).

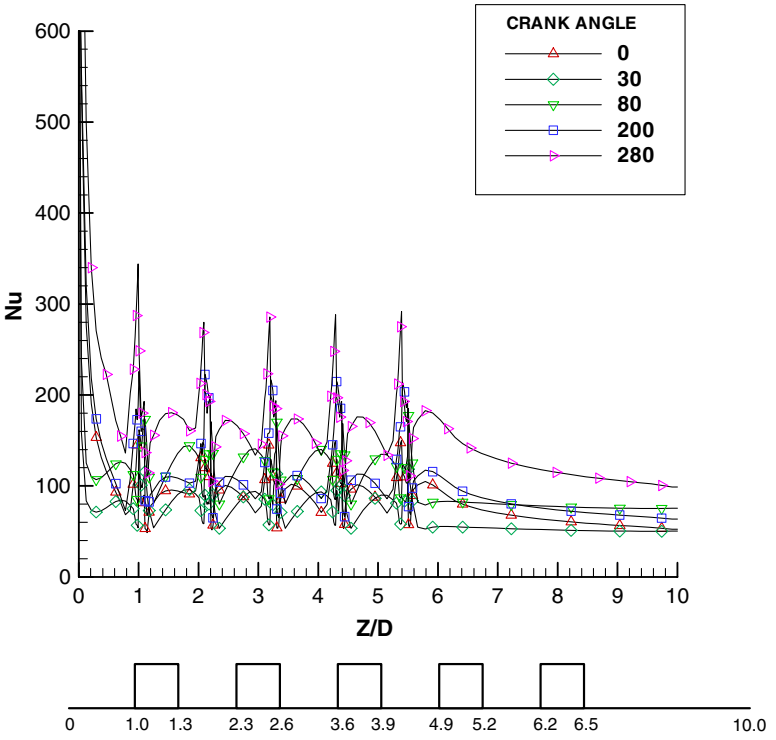

Fig. 8. Transient Nusselt number variation along channel wall for a reciprocating circular ribbed channel at $Pr = 7.0$, $Re = 5000$, $Gr = 400{,}000{,}000$, and $Pu = 6.2$ (60 rpm).

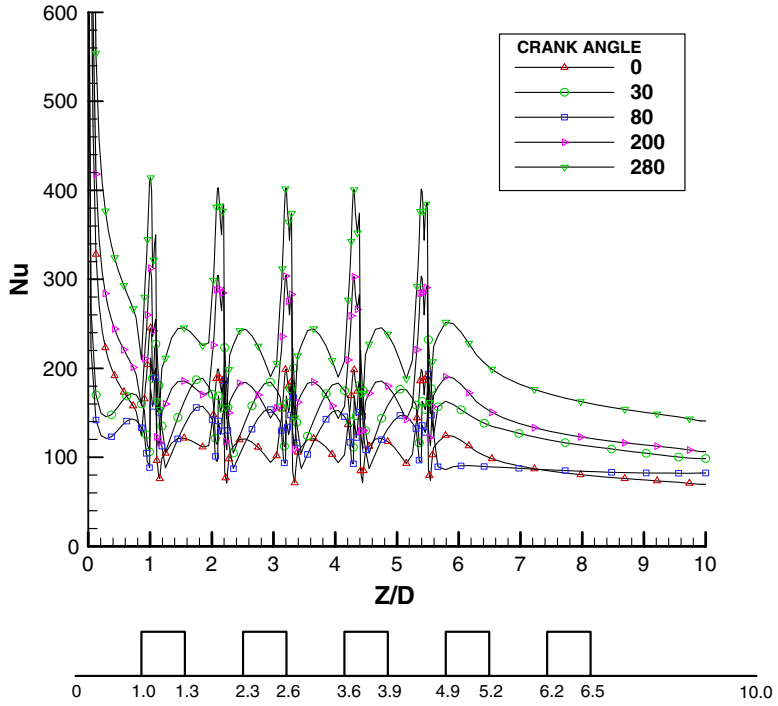

Fig. 9. Transient Nusselt number variation along channel wall for a reciprocating circular ribbed channel at $Pr = 7.0$, $Re = 10{,}000$, $Gr = 400{,}000{,}000$, and $Pu = 3.1$ (60 rpm).

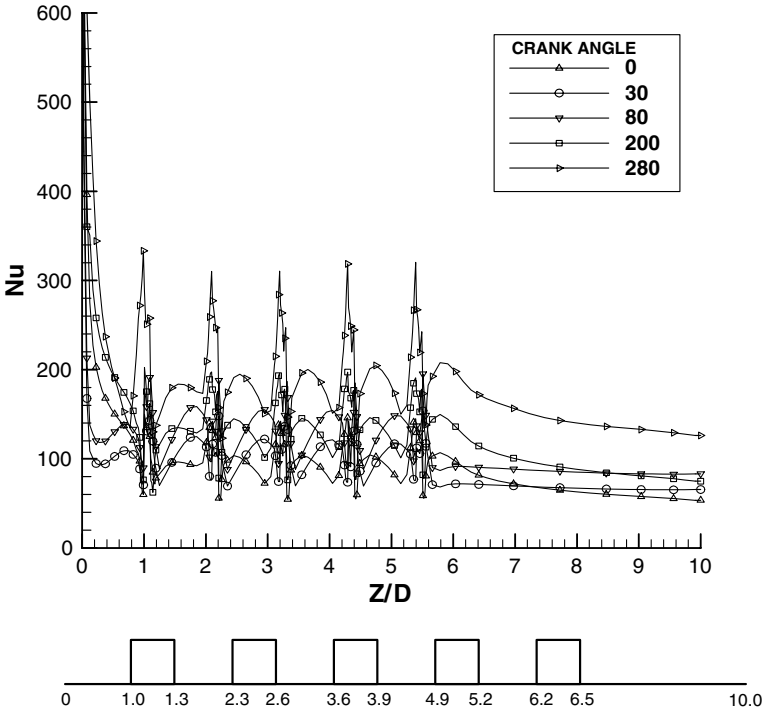

Fig. 10. Transient Nusselt number variation along channel wall for a reciprocating circular ribbed channel at $Pr = 84$, $Re = 4250$, $Gr = 0$, and $Pu = 3.1$ (60 rpm).

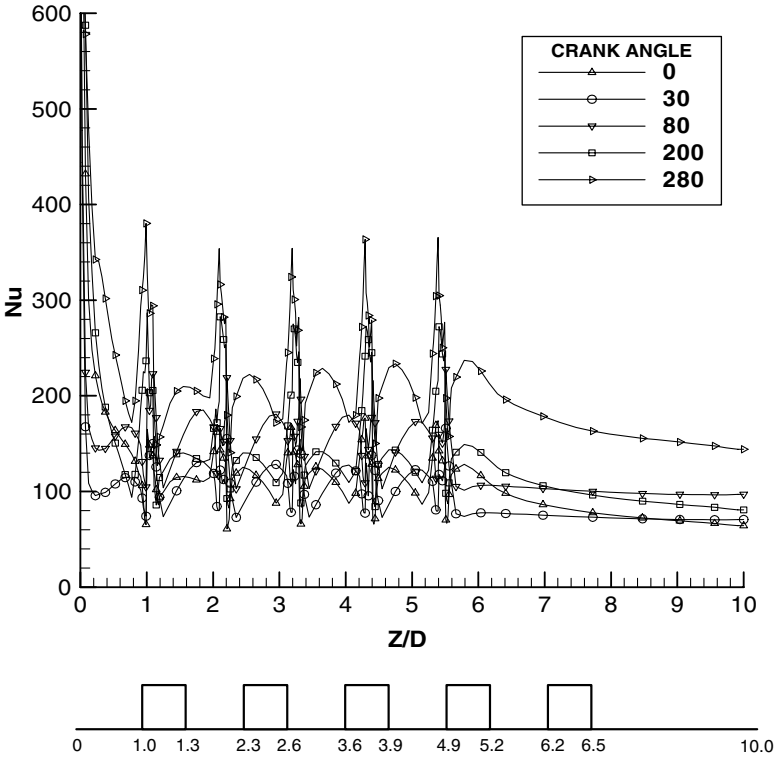

Fig. 11. Transient Nusselt number variation along channel wall for a reciprocating circular ribbed channel at $Pr = 84$, $Re = 4250$, $Gr = 0$, and $Pu = 4.64$ (90 rpm).

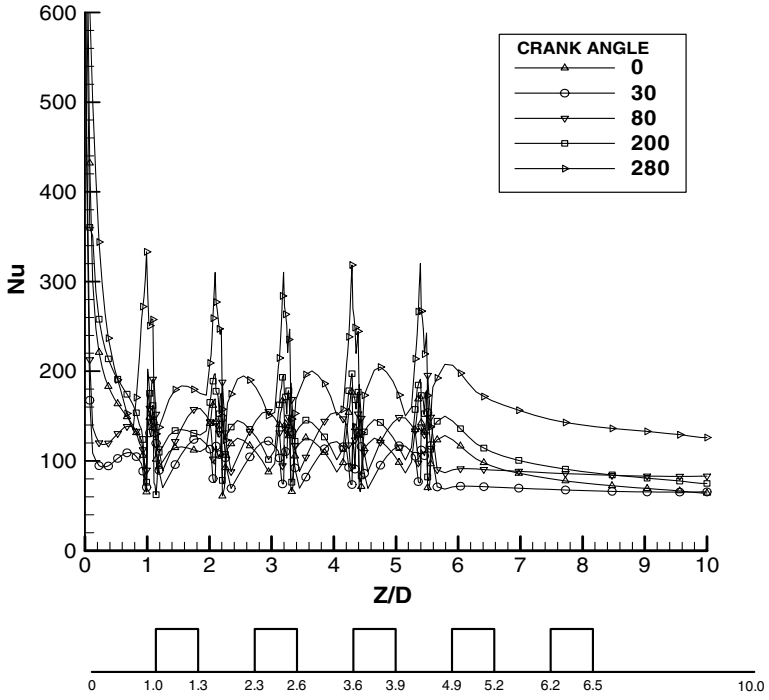

Fig. 12. Transient Nusselt number variation along channel wall for a reciprocating circular ribbed channel at $Pr = 84$, $Re = 4250$, $Gr = 400{,}000{,}000$, and $Pu = 3.1$ (60 rpm).

Table 2
The values of surface-and time-averaged Nusselt number for the channel wall with various values of Reynolds number, Grashof number and pulsating number for cooling water (gain denoting the increase percent to surface-and time- averaged Nusselt number for the stationary smooth channel at (panel A) $Re = 5000$; (panel B) $Re = 8{,}000$; (panel C) $Re = 10{,}000$)

	$\overline{Nu}_{ave}$	Gain (%)
Panel A		
$Re = 5000$, $\overline{Nu}_s = 45.6$		
Gr = 0		
Pu = 0	79.486	74.31
Pu = 3.1 (30 rpm)	82.099	80.04
Pu = 6.2 (60 rpm)	101.871	123.40
Pu = 9.3 (90 rpm)	128.642	182.11
Gr = 100,000,000		
Pu = 0	79.486	74.31
Pu = 3.1 (30 rpm)	84.937	86.26
Pu = 6.2 (60 rpm)	101.958	123.59
Pu = 9.3 (90 rpm)	128.654	182.14
Gr = 400,000,000		
Pu = 0	87.866	92.69
Pu = 3.1 (30 rpm)	86.394	89.46
Pu = 6.2 (60 rpm)	104.080	128.25
Pu = 9.3 (90 rpm)	128.745	182.34
Panel B		
$Re = 8000$, $\overline{Nu}_s = 66.41$		
Gr = 0		
Pu = 0	109.112	64.30
Pu = 1.94 (30 rpm)	115.800	74.37
Pu = 3.87 (60 rpm)	135.354	103.82
Pu = 5.80 (90 rpm)	167.686	152.50
Gr = 100,000,000		
Pu = 0	110.236	66.00
Pu = 1.94 (30 rpm)	116.785	75.86
Pu = 3.87 (60 rpm)	135.997	104.78
Pu = 5.80 (90 rpm)	167.757	152.61
Gr = 400,000,000		
Pu = 0	112.369	69.20
Pu = 1.94 (30 rpm)	118.462	78.38
Pu = 3.87 (60 rpm)	136.031	104.84
Pu = 5.80 (90 rpm)	167.984	152.95
Panel C		
$Re = 10{,}000$, $\overline{Nu}_s = 80.81$		
Gr = 0		
Pu = 0	117.370	45.24
Pu = 1.55 (30 rpm)	135.400	67.55
Pu = 3.1 (60 rpm)	154.236	90.86
Pu = 9.3 (90 rpm)	193.623	139.60
Gr = 100,000,000		
Pu = 0	117.562	45.48
Pu = 1.55 (30 rpm)	135.439	67.60
Pu = 3.10 (60 rpm)	154.275	90.91
Pu = 4.64 (90 rpm)	193.645	139.63
Gr = 400,000,000		
Pu = 0	122.894	52.08
Pu = 1.55 (30 rpm)	135.505	67.68
Pu = 3.10 (60 rpm)	154.341	90.99
Pu = 4.64 (90 rpm)	193.699	139.70

oil. For the water-cooling case ($Pr = 7.0$), the maximum value of surface-and time-averaged Nusselt number for the channel wall appears at $Re = 10{,}000$, $Gr = 400{,}000{,}000$ and $Pu = 4.64$ (90 rpm), because the interaction between larger reciprocating force and larger inlet fluid momentum can enhance the mix convection transfer. However, the maximum gain for the surface-and time-averaged Nusselt number is 182.34% occurring at $Re = 5000$, $Gr = 400{,}000{,}000$ and $Pu = 9.3$ (90 rpm); this is because of the small surface-and time-averaged Nusselt number for the equivalent smooth stationary case. An increasing proportion in the surface-and time-averaged Nusselt number reduces as the Reynolds number increases due to the pulsating number decreased for the same revolving speed. Increasing the surface-and time-averaged Nusselt number resulting from Grashof number increased at the fixed Reynolds number and pulsating number is only about 0.5–1%. As a result, some combinations of different Reynolds number, Grashof number and pulsating number can greatly increase the surface-and time-averaged Nusselt number so as to have

Table 3
The values of surface-and time-averaged Nusselt number for the channel wall with various values of Reynolds number, Grashof number and pulsating number for cooling oil (gain denotes the increase percent to surface-and time-averaged Nusselt number for the stationary smooth channel at $Re = 4250$)

	$\overline{Nu}_{ave}$	Gain (%)
$Re = 4250$, $\overline{Nu}_s = 54.2$		
Gr = 0		
Pu = 0	93.518	75.54
Pu = 1.55 (30 rpm)	101.764	87.76
Pu = 3.1 (60 rpm)	115.696	113.46
Pu = 9.3 (90 rpm)	135.392	149.80
Gr = 100,000,000		
Pu = 0	98.194	81.17
Pu = 1.55 (30 rpm)	102.763	89.60
Pu = 3.10 (60 rpm)	116.864	115.62
Pu = 4.64 (90 rpm)	135.498	150.00
Gr = 400,000,000		
Pu = 0	105.720	95.06
Pu = 1.55 (30 rpm)	107.763	98.83
Pu = 3.10 (60 rpm)	118.239	118.15
Pu = 4.64 (90 rpm)	136.194	151.28

a good effect in cooling performance for marine heavy engines. Under the same inlet velocity (Re = 10,000 for water and Re = 4250 for oil), the surface-and time-averaged Nusselt number for the oil-cooling case (Pr = 84) is much smaller than for the water-cooling case (Pr = 7.0) resulting from the smaller heat capacity *and larger fluid viscosity* for oil.

4. Conclusion

The unsteady turbulent mixed convection has been investigated in a circular ribbed channel under reciprocating motion by carrying out a numerical method. On the basis of these results presented and discussed in the discussion section, we draw the main conclusion as follows:

(1) The average time-mean Nusselt number gain for the reciprocating circular ribbed channel (relative to the equivalent stationary smooth case) can reach 45–182%.
(2) For the reciprocating circular ribbed channel, the surface-and time-averaged Nusselt number is found to increase with increasing both the Reynolds number and pulsating number due to the strong interaction between reciprocating force and inlet fluid momentum.
(3) For the reciprocating circular ribbed channel, the period of variation of Nusselt number decreases but the amplitude of oscillation increases with a pulsating number at the same Reynolds number due to a larger revolving speed.
(4) Buoyancy effect can help to enhance heat transfer for the stationary circular ribbed channel but this enhancement for the reciprocating ribbed channel goes down as the pulsating number increases.
(5) For the stationary or reciprocating circular ribbed channel, the averaged Nusselt number of oil-cooling case is lower than that of water-cooling case at the same incoming flow rate.

Acknowledgement

The authors gratefully acknowledge the financial support for this project by the National Science Council of the Republic of China under Grant no. NSC: 89–2611-E-006–063.

References

[1] J.B. Heywood, Internal Combustion Engine Fundamentals, McGraw-Hill Book Company, New York, 1988, pp. 36–37.
[2] M.K. Eberle, The marine diesel engine—the answer to low grade fuels, ASME Paper 80-DGP-16, 1980.
[3] S.W. Chang, L.M. Su, Influence of reciprocating motion on heat transfer inside a ribbed duct with application to piston cooling in marine diesel engines, J. Ship Res. 41 (4) (1997) 332–339.
[4] M. Mackley, G.M. Tweedle, I.D. Wyatt, Experimental heat transfer measurements for pulsatile flow in baffled tubes, Chem. Eng. Sci. 45 (5) (1990) 1237–1242.
[5] T.M. Howes, M.R. Mackley, Experimental axial dispersion for oscillatory flow through a baffled tube, Chem. Eng. Sci. 45 (5) (1990) 1349–1538.
[6] T. Fusegi, Numerical study of turbulent forced convection in a periodically ribbed channel with oscillatory throughflow, Int. J. Numer. Meth. Fluids 23 (11) (1996) 1223–1233.
[7] T. Fusegi, Mixed convection in a periodic open cavities with oscillatory throughflow, Numer. Heat Transfer, Part A 29 (1) (1996) 33–47.
[8] J.P. Van Doormaal, G.D. Raithby, Enhancements of the simple method for predicting incompressible fluid flows, Numer. Heat Transfer 7 (2) (1984) 147–163.
[9] B.E. Launder, D.B. Spalding, Numerical computation of turbulent flows, Comput. Meth. Appl. Mech. Eng. 3 (2) (1974) 269–289.
[10] W. Rodi, Experience with two-layer models combining the k–ε model with a one-equation model near the wall, in: AIAA-91-0216, Proc. 29th Aerospace Science Meet., Reno, NV, 1991, pp. 1–12.
[11] R.H. Sabersky, A.J. Acosta, E.G. Hauptmann, Fluid Flow—a First Course in Fluid Mechanics, third ed., Macmillan Publishing Company, New York, 1989, pp. 422–423.
[12] A. Bejan, Convective Heat Transfer, John Wiely, New York, 1984, pp. 113–114.
[13] R. Martinuzzi, A. Pollard, Comparative study of turbulence models in predicting turbulent pipe flow, AIAA J. 27 (1) (1989) 29–36.
[14] S.V. Pantankar, Numerical Heat Transfer and Fluid Flow, Hemisphere Publishing Corp., New York, 1980, pp. 102–104.
[15] L.H. Norris, W.C. Reynolds, Turbulent channel flow with a moving wavy boundary, Tech. Rep. FM-10, Department of Mechanical Engineering, Stanford University, 1975.
[16] R. Kiml, A. Magda, S. Mochizuki, A. Murata, Rib-induced secondary flow effects on local circumferential heat transfer distribution inside a circular rib-roughened tube, Int. J. Heat Mass Transfer 47 (6–7) (2004) 1403–1412.